RSC Advances

PAPER

View Article Online
View Journal | View Issue

Cite this: *RSC Adv.*, 2017, **7**, 50254

Structure, absolute configuration, and variable-temperature ^{1}H-NMR study of (±)-versiorcinols A–C, three racemates of diorcinol monoethers from the sponge-associated fungus *Aspergillus versicolor* 16F-11†

Bin-Bin Gu, Jie Tang, Shu-Ping Wang, Fan Sun, Fan Yang, Lei Li, Ying Xu and Hou-Wen Lin*

Three racemates of diorcinol monoethers, (±)-versiorcinols A–C (**1–3**), were initially isolated from the fungus *Aspergillus versicolor* 16F-11. The structures of versiorcinols B and C were elucidated by comprehensive spectroscopic analysis, while the structure of versiorcinol A was elucidated on the basis of quantum-chemical NMR chemical shifts, supported by DP4 probability analysis, and DU8 proton–proton spin–spin coupling constants (SSCCs) calculations in consortium with extensive experimental NMR analysis. The absolute configurations of the enantiomers (+)-**1** and (−)-**1**, (+)-**2** and (−)-**2**, and (+)-**3** and (−)-**3** were assigned from ECD calculations. At very low temperatures, the ^{1}H-NMR spectra of **1–3** revealed doubling of signals, which suggested the presence of two conformers in solution. Variable-temperature (VT) ^{1}H-NMR studies supported this hypothesis.

Received 1st June 2017
Accepted 13th October 2017

DOI: 10.1039/c7ra06106d

rsc.li/rsc-advances

Introduction

Fungi are widespread all over the world and have occupied almost every ecological niche, not only in terrestrial but also in freshwater and marine environments. For survival, secure access to living space and sufficient nutrition, fungi have developed a rich chemical ecology to survive the attacks of competitors and predators by the process of natural selection.[1] For instance, secondary metabolites serve chemical defense purposes, communication purposes, symbiotic interaction purposes, which have resulted in fungi as a promising reservoir for biologically and pharmaceutically active molecules attracting ever-growing studies.[2]

Phenyl ethers derived from a simple aromatic tetraketide orsellinic acid are a family of fungal metabolites that containing 5-methylbenzene-1,3-dioxy substructure. Their chemical diversity is attributed to: the number of orsellinic acid presented in these ethers (dimers in most cases and rare trimers);[3–12] differences in hydroxylation and decarboxylation of the orsellinic acid subunit;[3,4,6,9–12] multiformity of the ether bonds formed from phenolic hydroxyl groups;[3,6,8,10,11] differences in glycosylated and prenylated modifications;[3,5–8,13] and fusion of orsellinic acid derived units with other polyketide units,[10,14] such as C–C fusion of an anthraquinone and orcinol unit.[10] Among these structurally diverse orsellinic acid-derived phenyl ethers, diphenyl ethers were found to have various functions such as antiviral,[3] antibacterial,[4,7,9] anticancer,[5,6,8] antifungal,[15] acetylcholinesterase (AChE) inhibiting,[9] antioxidant,[10] osteoclastogenesis inhibiting,[16] and geranylgeranyl diphosphate synthase inhibiting[11] activities, and other orsellinic acid-derived phenyl ethers, such as F9775A and F9775B, were shown to have anti-osteoporosis activity.[17]

As part of our efforts for biological fungal metabolites, chemical investigations of fungi isolated from several marine sponges collected from Yongxing Island were initiated.[18,19] In the course of antibacterial activities-guided screening, a fungal strain *Aspergillus versicolor* 16F-11 (KM605199) isolated from marine sponge *Phakellia fusca* aroused our interest as the EtOAc extract of this fungal culture showed antibacterial activity against a panel of pathogenic bacteria. Our investigation of the EtOAc extract of the liquid fermentation of this fungus led to the discovery three racemates of diorcinol monoethers, (±)-versiorcinols A–C (**1–3**). Enantioseparations for (±)-**1**, (±)-**2**, and (±)-**3** were achieved on chiral HPLC to afford the enantiomers (+)-**1** and (−)-**1**, (+)-**2** and (−)-**2**, and (+)-**3** and (−)-**3**, respectively. The structures and absolute configurations of **1**, **2**, and **3** were unambiguously elucidated by high/low temperature 1D and 2D

Key Laboratory for Marine Drugs, Department of Pharmacy, State Key Laboratory of Oncogenes and Related Genes, Renji Hospital School of Medicine, Shanghai Jiao Tong University, Shanghai 200127, China. E-mail: franklin67@126.com

† Electronic supplementary information (ESI) available: Tables and figures giving HRESIMS, UV, IR, and 1D and 2D NMR spectra for compounds **1–3**, the low energy conformers for **a**, **b**, **c**, **2**, and **3**, the computed NMR chemicals shifts and SSCCs for **a** and **b**, the *in vitro* antibacterial activity of racemates (±)-**1**, (±)-**2**, and (±)-**3** and enantiomers (+)-**1** and (−)-**1**, (+)-**2** and (−)-**2**, and (+)-**3** and (−)-**3**, and atom coordinates of the computed structures. See DOI: 10.1039/c7ra06106d

NMR spectra (recorded at 80 °C in DMSO-d_6 for **1** and **3** and −40 °C in CD_3OD for **2**); DFT calculations of NMR chemical shifts, and ^{1}H NMR coupling constants; and time-dependent density functional theory (TDDFT) ECD calculations for solution conformers. Besides, the interesting phenomena of paired ^{1}H NMR signals of **1**, **2**, and **3** appeared at various low temperatures in the same solvent were investigated using VT ^{1}H-NMR study. Herein, we report the isolation, structural elucidation, VT ^{1}H-NMR study, and biological evaluation of these compounds.

Results and discussion

The fungus *A. versicolor* 16F-11 was cultivated on fungal liquid medium for 12 days. The crude EtOAc extract of the whole fermentation broth was fractionated by preparative medium pressure liquid chromatography (MPLC) followed by RP-HPLC chromatography to yield (±)-versiorcinol A–C (**1–3**, Fig. 1).

(±)-Versiorcinol A (**1**) has a molecular formula of $C_{22}H_{20}O_5$ provided by the positive HRESIMS (*m*/*z* 365.1371 $[M + H]^+$, calcd 365.1389), which indicated thirteen double-bound equivalents in the molecule. The IR spectrum of **1** displayed absorptions for hydroxyl (3327 cm^{-1}) group(s) and aromatic ring(s) (1700, 1594, 1468 cm^{-1}). As several carbon signals were broadened and disappeared at 25 °C and improved and emerged at 80 °C in DMSO-d_6 (ESI, Fig. S7 and S8†), we rerecorded the 1D and 2D NMR spectra of **1** at 80 °C in DMSO-d_6. The ^{1}H NMR spectrum of compound **1** (Table 1) showed: eight aromatic protons, three of which were apparently characterized by a first-order ABC coupling system (δ_H 6.68, 7.04, and 6.57); two diastereotopic oxygenated methylene protons (δ_H 5.16, 4.98); one oxygen-bearing methine proton (δ_H 6.63), and two methyl protons most probably attached to aromatic ring(s) (δ_H 2.01, 2.19). Its ^{13}C NMR and DEPT spectra (Table 1) exhibited a total of 22 carbon resonances divided into 10 sp^2 quaternary carbon atoms (5 oxygenated quaternary carbons, 5 quaternary carbons) and 8 sp^2 methines at low field and 4 sp^3 carbon atoms at high field (1 sp^3 methine, 1 sp^3 methylene, and 2 methyls), accounting for nine double-bond equivalents. The remaining four degrees of unsaturation is due to the presence of four rings in its molecule. The HSQC cross peaks facilitated the assignment of the protons to the corresponding carbon atoms. A consecutive ^{1}H–^{1}H COSY correlation from H-4 to H-6, together with the HMBC correlations form aromatic H-4 (δ_H 6.68, dd, J = 7.0, 0.6 Hz) and H-6 (δ_H 6.57, dd, J = 7.9, 0.6 Hz) to C-2 (δ_C 126.8), from H-6 and H-5 (δ_H 7.04, t, J = 7.6 Hz) to C-1 (δ_C 151.7), from H-5 to C-3 (δ_C 141.4), from oxygenated methylene H_2-8 (δ_H 5.16, dd, J = 11.9, 3.0 Hz; 4.98, d, J = 11.9 Hz) to C-2, C-3, C-4 (δ_C 110.7), and C-7 (δ_C 77.5), from oxygenated methine H-7 (δ_H 6.63, brt, J = 2.8 Hz) to C-2 could establish the 3,4-disubstituted 1,3-dihydroisobenzofuran moiety, the A and B rings (Fig. 2). Moreover, the magnitude of C-1 carbon chemical shift (δ_C 151.7) hinted that an oxygen atom is positioned at C-1. The rest ^{1}H and ^{13}C NMR resonances of **1**, two methyls, five aromatic methines (δ_H 6.23, d, J = 2.4 Hz; 6.17, d, J = 2.3 Hz; 6.18, t, J = 2.2 Hz; 6.25, m; 6.33, m), and four oxygen-bearing sp^2 quaternary carbons (156.9, 155.8, 158.1, and 157.2), highlighted that **1** contains two additional benzene rings, the ring C (tetra-substituted) and the D ring (tri-substituted), which was reinforced by HMBC correlations of H-7′/C4′ and C6′, H-2′/C4′ and C6′, H-4′/C6′, H-7″/C4″ and C6″, H-2″/C4″ and C6″, and H-4″/C6″. The HMBC correlations of H_2-8 with C6′ (δ_C 120.4) and of H-7 with C1′ (δ_C 156.9), C5′ (139.1), and C6′ allowed a connection of ring C and the aforementioned 3,4-disubstituted 1,3-dihydroisobenzofuran moiety to form the A/B/C fragment *via* a C–C bond (C7–C6′). However, the final ether linkage site, between ring D and the A/B/C, is uncertain (the shortest bond distance (H→C) between ring D and A/B/C is 4-bond) and leaving it open as to whether the ether bond is formed between C1′ (156.9) and C1″ (**a**, Fig. 2) or between C3′ (155.8) and C1″ (**b**, Fig. 2) or between C1 (151.7) and C1″ (**c**, Fig. 2) as no ^{1}H/^{13}C correlation(s) between ring D and A/B/C could be found in the HMBC spectrum (Fig. 2 and ESI, Fig. S21†). Initial proofreading the experimental NOEs with the spatial locations of the corresponding hydrogens in the most stable conformers of structures of **a**, **b**, and **c** (Fig. 2), however, ruled out the candidate structure **c**, because H-7′ (δ_H 2.01) and H-8 (δ_H 5.16) are at the opposite side of A/B plane in **c** and no NOE effect could be observed (see ESI, Fig. S1,† in any and every of all the low-energy conformers of **c**, H-7′ and H-8 (δ_H 5.16) are on the opposite face of the A/B ring). Finally, for ruling out candidate structure and supporting the correct one for the single stereocenter-containing compound **1**, a solution was secured by computation, including DFT calculations accurate NMR chemical shifts and ^{1}H NMR coupling constants.

With improvements in accuracy and affordability, computational modeling of ^{1}H and ^{13}C chemical shifts by *ab initio* methods based on gauge including atomic orbital (GIAO)[20] have found increased utility in natural product assignments.[21] In this

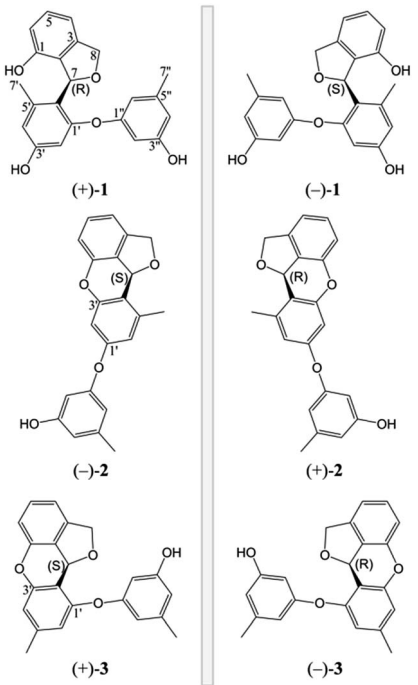

Fig. 1 Structures of versiorcinols A–C (**1–3**).

Table 1 ^{1}H (600 MHz) and ^{13}C (150 MHz) NMR spectroscopic data of versiorcinols A–C (**1**–**3**)

			2[b]					
	1[a]		Conformer **A**[c] (58.2%)		Conformer **B**[c] (41.8%)		**3**[a]	
Position	δ_H (J in Hz)	δ_C	δ_H (J in Hz)	δ_C	δ_H (J in Hz)	δ_C	δ_H (J in Hz)	δ_C
1		151.7		153.3		153.7		151.5
2		126.8		127.5		127.2		126.9
3		141.4		142.4		142.4		141.6
4	6.68, dd (7.0, 0.6)	110.7	6.50, m	111.9	6.75, m	112.5	6.55, d (7.4)	110.3
5	7.04, t (7.6)	128.1	6.92, t (7.7)	129.7	7.13, t (7.7)	130.4	6.94, t (7.7)	127.6
6	6.57, dd (7.9, 0.6)	113.5	6.50, m	113.9	6.60, d (7.9)	114.5	6.52, d (7.9)	113.1
7	6.63, brt (2.8)	77.5	6.56, d (2.4)	81.2	6.75, m	79.4	6.59, d (2.5)	75.7
8	5.16, dd (11.9, 3.0)	72.3	5.15, dd (11.3, 2.9)	75.2	5.23, dd (11.9, 2.3)	73.9	5.02, dd (11.5, 3.1)	72.7
	4.98, brd (11.9)		5.01, d (11.2)		5.10, dd (12.0, 2.6)		4.87, d (11.4)	
1′		156.9		158.6		158.8		156.8
2′	6.23, d (2.4)	103.3	6.00, d (2.2)	106.1	6.11, d (2.3)	104.9		116.8
3′		155.8		158.6		157.9		155.6
4′	6.17, d (2.3)	111.2		123.1		121.7	6.02, m	110.3
5′		139.1		140.5		142.1		137.5
6′		120.4	6.39 d (2.1)	113.1	6.30, m	115.1	6.35, brs	111.5
7′	2.01, s	18.9	2.53, s	20.7	1.84, s	19.6	2.10, s	20.4
1″		158.1		159.8		160.7		158.2
2″	6.18, t (2.2)	102.9	5.84, brs	103.2	6.30, m	103.8	6.02, m	102.2
3″		157.2		159.0		159.5		157.6
4″	6.25, m	109.8	6.15, brs	110.9	6.31, brs	111.3	6.02, m	109.1
5″		139.5		140.8		141.4		138.8
6″	6.33, m	110.9	5.79, brs	110.7	6.37, brs	111.3	6.22, brs	110.0
7″	2.19, s	20.6	2.09, s	21.6	2.23, s	21.7	2.11, s	20.6

[a] In DMSO-d_6 at 80 °C. [b] In CD_3OD at −40 °C. [c] These percents were estimated based upon the ratio of integral areas of H-7′ of conformer **A** to H-7′* of conformer **B** in the ^{1}H NMR spectrum.

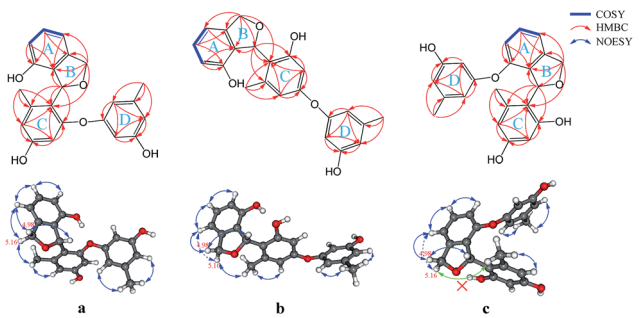

Fig. 2 Key 2D NMR correlations of three possible structures (**a**, **b**, and **c**) of **1**. No NOESY correlation could be found between H-7′ (δ_H 2.01) and H-8 (δ_H 5.16) in **c** (the green arrow).

event, the initial MMFF conformational search of **a** and **b** resulted in, respectively, 91 and 93 stable conformers in a 21 kJ mol^{-1} energy window. These stable conformers for **a** and **b** were optimized by DFT calculations at the B3LYP/6-31G(d) level with the PCM solvent model for DMSO. Then, the thereby yielded 62 and 63 conformers (ESI, Tables S1 and S2†), respectively, were subjected to NMR chemical shifts calculations at the B3LYP/6-311+G(2d,p) level with the PCM solvent model for DMSO.[21] The theoretical NMR chemical shifts for **a** and **b** were estimated from calculated chemical shifts for each of the stable conformers for **a** and **b** weighted to their Boltzmann distribution (B3LYP/6-31G(d), PCM/DMSO, 353.15 K). Both ^{1}H and ^{13}C NMR chemical shifts of **1** showed better overall agreement with the theoretical NMR chemical shifts for **a** than those for **b** (CMAE: 1.2 *vs.* 1.6 ppm for ^{13}C, 0.07 *vs.* 0.10 ppm for ^{1}H; R^2: 0.998 *vs.* 0.996 for ^{13}C, 0.996 *vs.* 0.994 for ^{1}H; Fig. 3 and ESI, Fig. S2 and S3 and Table S3†). This comparison was also judged by DP4 probability, using t distribution and DP4-database 2.[22,23] DP4 analysis identified **a** as the real structure of versiorcinol A (**1**) from two possible structures (**a** and **b**) with a probability of 100.0% (using both carbon and proton data; 0.0% for **b**).

Accurate and rapid computations of proton SSCC are particularly attractive as SSCCs carry a plethora of structural information helping to inform and guide the structural assignment of complex organic molecules. In 2015, Kutateladze and Mukhina improved the SSCC calculation based on parametric scaling of the DFT-computed Fermi contacts (FCs), extended by a "minimalistic relativistic force field" (DU8) that utilized the natural bond order (NBO) hybridization coefficients for parametric scaling, requiring only four general types of SSCCs.[24] The (wall) time for running a individual conformer of **a** size on a single 4-core Linux node does not exceed 1 h and yet gives 0.4 Hz rmsd, which is usually sufficient for unambiguous structural assignment.

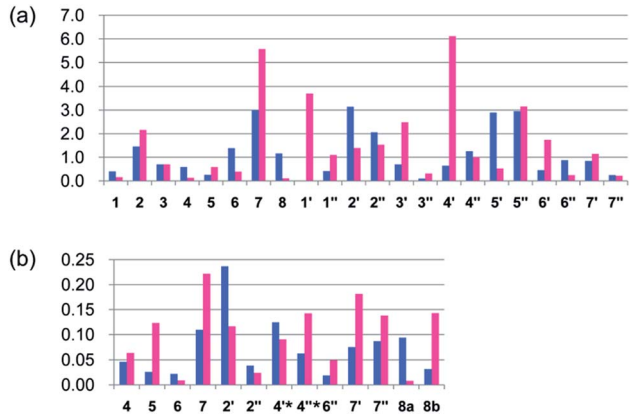

Fig. 3 Differences between NMR chemical shifts of versiorcinol A (**1**) and theoretical NMR chemical shifts for **a** (blue bar) and **b** (red bar). (a) $\Delta\delta_C$ (in ppm) = δ_C of **1** (150 MHz in DMSO-d_6) − δ_C of **a** (blue bar) or **b** (red bar). (b) $\Delta\delta_H$ (in ppm) = δ_H of **1** (600 MHz in DMSO-d_6) − δ_H of **a** (blue bar) or **b** (red bar). The horizontal and vertical axes represent atom numbers of **a**/**b** and $\Delta\delta$ value [$\Delta\delta$ (in ppm) = δ of **1** − δ of **a** (blue bar) or **b** (red bar)], respectively. Protons with "*" are nuclei H-4′ and H-4″ in structure **a** (blue bar) but, correspondingly, H-4″ and H-6′ in structure **b** (red bar).

The geometries of conformers of **a** and **b** were first optimized using B3LYP/6-31G(d) PCM/DMSO level of theory, followed by calculation of SSCCs of each conformer using DU8 basis set[24b] (ESI, Table S5†). Energies of each of the 62 stable conformers of **a** and 63 stable conformers of **b** were calculated (B3LYP/6-31G(d) or B3LYP/6-311+G(2d,p), PCM/DMSO, 353.15 K) and the correspondingly theoretical SSCCs of **a** and **b** were acquired after weighting by the Boltzmann populations of the associated conformers.[21] As expected (ESI, Table S5† and Fig. 4), all the corresponding ΔJ values of the aromatic parts of **a** and **b** are very close (not exceeding 0.4 Hz) and the different locations of D ring in **a** and **b** affect most the couplings between H-7 and H_2-8 (with the ΔJ values of $^4J_{H7-H8b}$ and $^4J_{H7-H8a}$ about 0.7 and 0.7 Hz for **a** and 1.1 and 1.4 Hz for **b**, respectively). Again, **a** matched more closely (rmsd: 0.4 Hz for **a** *vs.* 0.7 Hz for **b**) with the measured values of **1** (ESI, Table S5†).

Taken collectively, our computational evidences strongly suggest that **a** is the true structure of **1**.[25] Fig. 5 illustrates how well its multiplets are simulated with the computed SSCCs of **a**.

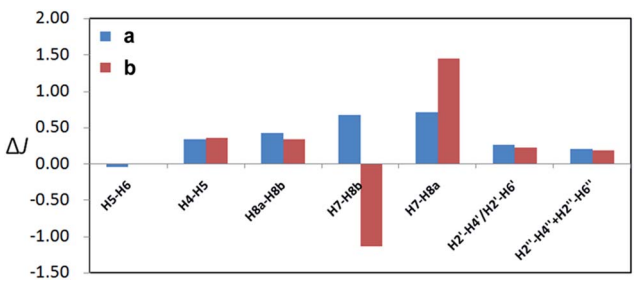

Fig. 4 Calculated (DFT optimized geometries, DU8 basis set, and B3LYP/6-31G(d) relative free energies at 353.15 K for Boltzmann distributions; see ref. 24*b*, text, and ESI, Table S5†) coupling constants differences (ΔJ) of **a** and **b** from experimental values of versiorcinol A (**1**).

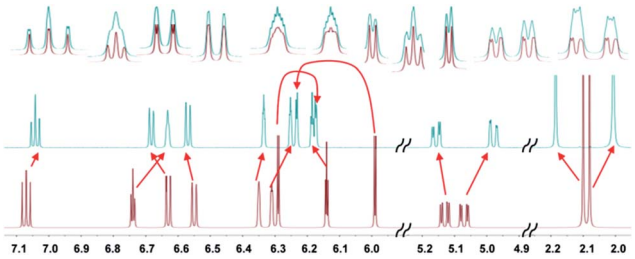

Fig. 5 Experimental (top) and simulated NMR spectra for versiorcinol A (**1**); using the linearly corrected chemical shifts (ESI, Table S3†) mentioned above (all the calculated coupling constants and ^{1}H chemical shifts were Boltzmann distributed using the B3LYP/6-31G(d) ΔG energy).

The lack of optical activity indicated the racemic nature of **1**. Following resolution for **1** was tackled by an enantioseparation procedure ((+)-**1** and (−)-**1** in a ratio of almost 1 : 1) (ESI, Fig. S63†). The observation of opposite optical rotation values and mirror ECD spectra for (+)-**1** and (−)-**1** confirmed their enantiomeric relationship (Fig. 6).

The absolute configurations of (+)-**1** and (−)-**1** were determined by TDDFT ECD calculation. The B3LYP/6-31G(d) PCM/MeOH reoptimization of the 91 MMFF conformers of (7*R*)-**1** yielded 14 conformers above 1% (ESI, Tables S6 and S7 and Fig. S4†). The resulted theoretical ECD spectrum were in fairly good agreement with the experimental ECD spectrum for (+)-**1** (Fig. 6). Therefore, 7*R* and 7*S* were finally assigned for (+)-**1** and (−)-**1**, respectively.

(±)-Versiorcinol B (**2**) has a molecular formula of $C_{22}H_{18}O_4$, with 14 degrees of unsaturation, one more degree of unsaturation and 18 less mass units (H_2O) than in (±)-versiorcinol A (**1**), as established by HRESIMS (*m*/*z* 347.1266 $[M + H]^+$, calcd 347.1283). The IR spectrum also suggested the presence of hydroxyl group(s) (3329 cm^{-1}) and aromatic ring(s) (1700, 1599, 1468 cm^{-1}). As the ^{1}H NMR spectra of compound **2** were severely broadened and distorted at 25 °C and improved

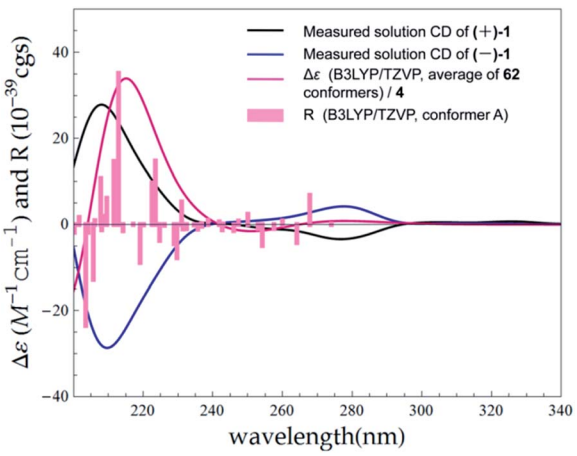

Fig. 6 Experimental ECD spectra of (+)-**1** and (−)-**1** in MeOH compared with the Boltzmann-weighted B3LYP/TZVP (PCM/MeOH) spectrum calculated for (7*R*)-**1**. Bars represent rotational strength of the lowest energy conformer.

tremendously at 80 °C in DMSO-d_6 (ESI, Fig. S10 and S11†), we thus registered the 1D and 2D NMR spectra of **2** at 80 °C in DMSO-d_6. However, several carbon signals were still broadened. As a consequence, a few key HMBC correlations were unexposed in its HMBC spectrum. Then, we resorted to cryogenic NMR experiments. Pre-examination the ^{1}H NMR spectra of **2** (dissolved in CD_3OD) showed that when the temperature dropped to −20 °C, two sets of well-distinguished peaks were emerged and, moreover, this distinctiveness and the shape of peaks were further improved at −40 °C (ESI, Fig. S12†). Accordingly, we rerecorded the 1D and 2D NMR spectra of **2** at −40 °C in CD_3OD as well. An initial study of the ^{1}H NMR data (Table 1) revealed a doubling of all the signals with a nearly 1.39 : 1.00 ratio. We attributed this phenomenon to the presence of two conformers in a 1.39 : 1.00 ratio at −40 °C in CD_3OD. Comparing the ^{1}H and ^{13}C NMR spectra of **2** with those of **1** showed that they are almost identical, with the exception that there are very small deviations in the values of chemical shifts and coupling constants (Table 1), which suggested, as in **1**, these ^{1}H and ^{13}C NMR data also encompass nine degrees of unsaturation. The remaining five indices of hydrogen deficiency indicated **2** is a pentacyclic compound (one more ring than in **1**). Detailed analyses of the ^{1}H–^{1}H COSY, HMBC, and ROESY correlations (Fig. 7) disclosed that **2** also has a 3,4-disubstituted 1,3-dihydroisobenzofuran scaffold, the A and B rings, and a 4/6-substituted diorcinol unit, the C and D rings, being edited into the molecule according to key HMBC correlations of H_2-8 with C4′ (δ_C 123.1) and of H-7 with C3′ (δ_C 158.6), C4′, and C5′ (140.5) (cluster **A**, 58.2%, Table 1). It remained to assign a single oxygen to accommodate the last ring in **2**. Based on geometric considerations and 18 mass units (H_2O) less than in **1**, it could only be explained by assuming an ether bond formed between C1 and C3′ (Fig. 7).

The MMFF conformational search resulted in 35 conformers for (7*S*)-**2**, which were reoptimized at the B3LYP/6-31G(d) with PCM model for MeOH level, yielding 22 conformers above 1% (ESI, Tables S6 and S8 and Fig. S5†). The Boltzmann-averaged ECD spectrum for (7*S*)-**2** reproduced well the two ECD transitions of the experimental spectrum of (−)-**2**, enabling the unambiguous assignments of the 7*R* and 7*S* absolute configurations for (+)-**2** and (−)-**2**, respectively (Fig. 8).

(±)-Versiorcinol C (**3**), which also consists of a pair of enantiomers, has the same molecular formula of $C_{22}H_{18}O_4$ as **2** (HRESIMS *m*/*z* 347.1266 $[M + H]^+$, calcd 347.1283). As the situation in **1** and **2**, several carbons were disappeared at 25 °C and emerged at 80 °C in DMSO-d_6 (ESI, Fig. S13 and S14†), we then registered the 1D and 2D NMR spectra of **3** at 80 °C in DMSO-d_6.

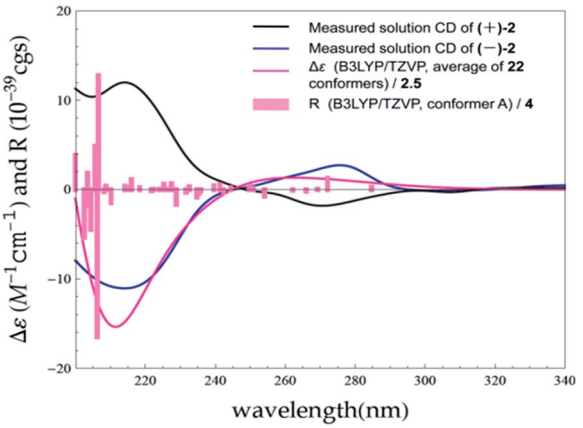

Fig. 8 Experimental ECD spectra of (+)-**2** and (−)-**2** in MeOH compared with the Boltzmann-weighted B3LYP/TZVP (PCM/MeOH) spectrum calculated for (7*S*)-**2**. Bars represent rotational strength of the lowest energy conformer.

Detailed comparison of its NMR data with those of **2** indicated that the only difference between **3** and **2** is the small deviation of the values of chemical shifts and coupling constants (Table 1), which suggested that **3** has a 3,4-disubstituted 1,3-dihydroisobenzofuran moiety (A and B rings) and a diorcinol moiety (C and D rings) as well, being corroborated by the ^{1}H–^{1}H COSY, HMBC, and NOESY correlations (Fig. 9). The discerned key HMBC correlations of H_2-8 with C2′ (δ_C 116.8) and of H-7 with C1′ (δ_C 156.8), C2′, and C3′ (δ_C 155.6) manifested the connection of these two moieties *via* the C7–C2′ bond. Based on geometric considerations, the ring E, formed through the formation of an ether bond between C1 and C3′, was assigned to accommodate the last degree of unsaturation and complete the structure of **3**.

The initial MMFF conformational search of (7*S*)-**3** resulted in 24 conformers. The B3LYP/6-31G(d) PCM/MeOH optimization of these conformers yielded 17 conformers above 1% (ESI, Tables S6 and S9 and Fig. S6†). The overall ECD spectrum for (7*S*)-**3** is in good accordance with the experimental ECD for (+)-**3** (Fig. 10). Therefore, the absolute configurations of (+)-**3** and (−)-**3** were designated as 7*S* and 7*R*.

The ^{1}H- and ^{13}C-NMR spectra of **2** at −40 °C in CD_3OD revealed doubling of signals, which suggested the presence of two conformers in solution separated by a relatively high energy barrier. To support this hypothesis, VT ^{1}H-NMR study was conducted for compounds **1–3**.

As shown in Fig. 11–13, the ^{1}H NMR spectra of **1–3** at different temperatures in CD_3OD, ranging from −60 °C to 60 °C, were recorded. At 25 °C, the ^{1}H NMR of **1** and **3** displayed sharp

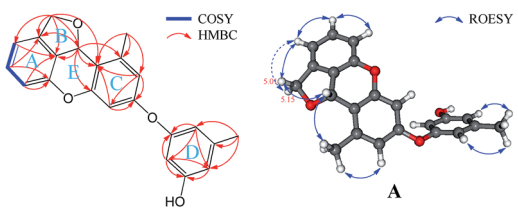

Fig. 7 Key 2D NMR correlations of **2**.

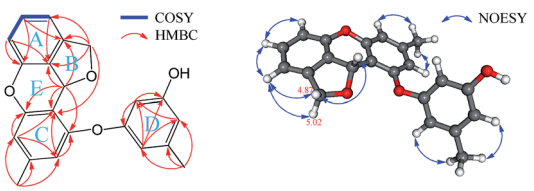

Fig. 9 Key 2D NMR correlations of **3**.

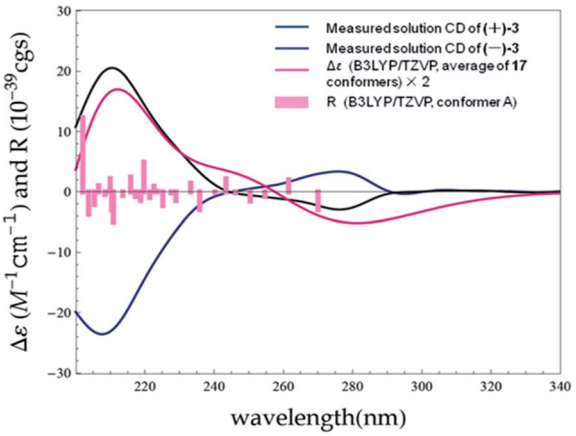

Fig. 10 Experimental ECD spectra of (+)-**3** and (−)-**3** in MeOH compared with the Boltzmann-weighted B3LYP/TZVP (PCM/MeOH) spectrum calculated for (7*S*)-**3**. Bars represent rotational strength of the lowest energy conformer.

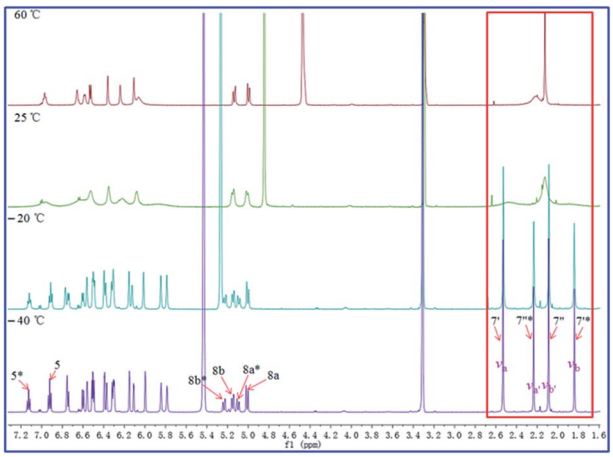

Fig. 12 Effect of temperature on the ^{1}H NMR spectra of compound **2** in CD_3OD.

and well *J*-coupling splitted peaks (Fig. 11 and 13), while in the ^{1}H NMR of **2**, the whole ^{1}H NMR spectrum was broadened seriously (Fig. 12), which even let us suspect whether we got the pure form of **2** before. When the measurement temperature raised to 60 °C, all the originally unresolved peaks of **2** were emerged, though with "apparently simple" peak pattern, indicating that this low-resolved peak pattern could be further refined and finally resolved as the temperature grows if possible (the boiling point of MeOH is 64.7 °C), whereas the ^{1}H NMR spectra of **1** and **3** had almost no change. On the contrary, when the temperature dipped to −20 °C, several peaks of **1** were disappeared, while the other peaks of **1** were broadened in varying degrees; all of the proton signals in **3** were just broadened (with varying degrees); two sets of well-discriminated peaks of **2** in a nearly 1.39 : 1.00 ratio were well resolved. The discrimination of the paired signals as well as the splitting and shape of the relevant peaks of **2** were further refined at −40 °C. However, the trend for forming paired signals of **1** lagged behind that of **2**. As shown in Fig. 11, the paired signals of **1** (1.19 : 1.00) were appeared and well-resolved till the temperature was dropped to −60 °C. For **3**, even at −60 °C (Fig. 13), the ^{1}H NMR spectrum was yet broadened, with the beginning of the sign of paired signals being discerned for the methyl group at 2.0–2.2 δ_H (1.79 : 1.00; because of the lowest-temperature limitation of our available NMR probe, we didn't record ^{1}H NMR spectra of **3** at lower temperatures than −60 °C).

For compound **1** (Fig. 11), using the H_3-7′ signals as a marker, two conformers were in slow exchange at −60 °C, therefore, two absorptions for this methyl group were individually detected. At −40 °C, conformational exchange was fast enough for time averaging to cause broadening of these two absorptions. At −20 °C, the increased rate of exchange has caused a initial coalescence of the methyl signals at *ca.* 2.12 ppm. At 25 °C, the methyl signal has sharpened dramatically. Thus the coalescence temperature (T_C) of this methyl was slightly higher than −20 °C. This coalescence of signals was noticed for the entire ^{1}H NMR spectrum, although the other

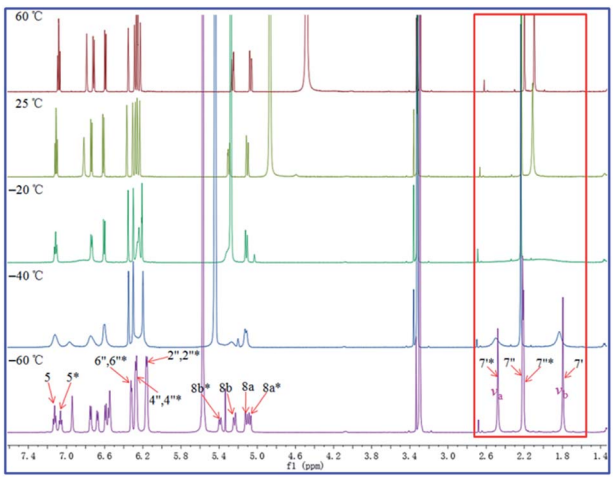

Fig. 11 Effect of temperature on the ^{1}H NMR spectra of compound **1** in CD_3OD.

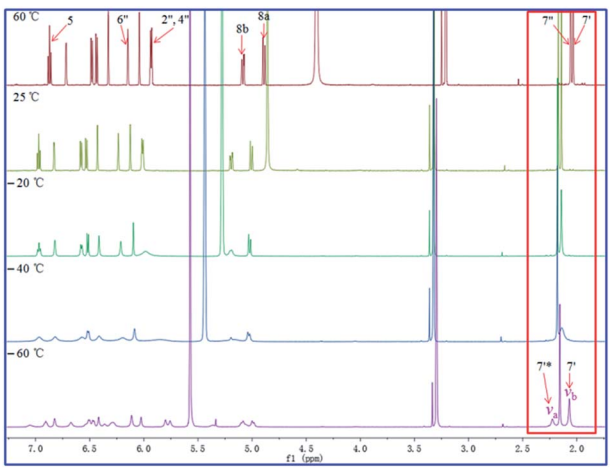

Fig. 13 Effect of temperature on the ^{1}H NMR spectra of compound **3** in CD_3OD.

pairs of signals coalesced at lower temperatures manifesting their smaller chemical shift differences. For compound **2** (Fig. 12), we used H_3-7′ and H_3-7″ signals as markers. And the two signals for H_3-7″ coalesced to a single peak at *ca.* 2.13 ppm at a T_C of 25 °C, while the two signals for H_3-7′ coalesced to a single peak at *ca.* 2.21 ppm at a T_C of 60 °C. For compound **3** (Fig. 13), using the H_3-7′ signals as a marker, at a T_C of −40 °C, the two signals for this methyl group coalesced to a single peak at *ca.* 2.14 ppm.

The free energies of activation for the interconversion between the two unequally populated conformers of versiorcinol A (**1**), versiorcinol B (**2**), and versiorcinol C (**3**) can be calculated using the modified Eyring's equations (**a** and **b**):[26] $\Delta G_A^{\ddagger} = 4.57T_C\{10.62 + \log[X/2\pi(1 - \Delta P)] + \log(T_C/\Delta\nu)\}$ (**a**) and $\Delta G_B^{\ddagger} = 4.57T_C\{10.62 + \log[X/2\pi(1 + \Delta P)] + \log(T_C/\Delta\nu)\}$ (**b**), where $X = 2\pi\tau\Delta\nu$ and $\Delta P = P_A - P_B$. P_A and P_B represent the population of the conformers **A** and **B** ($P_A > P_B$, $P_A + P_B = 1$), respectively, τ is the mean lifetime, T_C is the coalescence temperature, and $\Delta\nu$ is the chemical shift difference between the two lines expressed in Hz ($\nu_a - \nu_b$). X is obtained using equation (**c**): $P_A - P_B = \Delta P = [(X^2 - 2)/3]^{3/2} \times 1/X$.

From the ^{1}H NMR spectrum of **1** at −60 °C (213 K), the frequency difference, $\Delta\nu$, between the H_3-7′ signals was 409.2 Hz and the T_C of this H_3-7′ group in **1** was slightly higher than −20 °C (253 K). Thereby, the $\Delta G_A^{\ddagger}$ and $\Delta G_B^{\ddagger}$ values should be slightly larger than 11.7 and 11.8 kcal mol^{-1}, respectively. For compound **2**, using the H_3-7″ signals as a marker, the $\Delta G_A^{\ddagger}$ and $\Delta G_B^{\ddagger}$ were respectively calculated as 14.8 and 15.0 kcal mol^{-1} ($\Delta\nu$ = 87.0, T_C = 25 °C (298 K)); when the H_3-7′ signals was used as a marker, these two values were 15.5 and 15.8 kcal mol^{-1}, respectively ($\Delta\nu$ = 415.2, T_C = 60 °C (333 K)). Finally, for compound **3**, the $\Delta G_A^{\ddagger}$ and $\Delta G_B^{\ddagger}$ were calculated as 11.3 and 11.7, respectively, when the H_3-7′ signals were employed as a marker ($\Delta\nu$ = 94.2, T_C = −40 °C (233 K)). Accordingly, we approximately estimated the $\Delta G^{\ddagger}$ about 12.0, 15.0, and 11.0 kcal mol^{-1} for **1**, **2**, and **3**, respectively.

The VT ^{1}H-NMR study confirmed the hypothesis that each appearance of doubled signals in the ^{1}H NMR spectra of **1**, **2**, and **3** was due to the presence of two conformers in solution separated by a relatively high energy barrier. Besides, the relative sizes of numerical magnitudes of $\Delta G^{\ddagger}$ for **1**, **2**, and **3** are in accordance with the relative temperature levels for showing paired signals in their ^{1}H NMR spectra.

In the cases of the bioactivities, *in vitro* cytotoxic activity evaluation for racemates (±)-**1**, (±)-**2**, and (±)-**3** and enantiomers (+)-**1** and (−)-**1**, (+)-**2** and (−)-**2**, and (+)-**3** and (−)-**3** was performed indicating that none of them displayed cytotoxicity toward MCF-7 and U937 cell lines even after 72 h treatments at the highest dose of 20 μmol L^{-1} (μM). For antibacterial activity testing (ESI, Table S10†), however, the racemate (±)-**1** and enantiomers (+)- and (−)-**1** showed medium antibacterial activity against *Staphylococcus aureus* (32, 32, and 16 μg mL^{-1}, respectively), methicillin-resistant *Staphylococcus aureus* (64, 64, and 32 μg mL^{-1}, respectively), and *Enterococcus faecalis* C1129 (64, 64, and 32 μg mL^{-1}, respectively); no antibacterial activity against *Escherichia coli*, *Salmonella typhimurium* SL1344, *Acinetobacter baumanii* ATCC19606, and *Klebsiella pneumoniae* ATCC13883 was observed (MIC > 64 μg mL^{-1}).

Conclusions

We reported three racemates of diorcinl monoethers, (±)-versiorcinols A–C (**1–3**), isolated from the marine sponge *P. fusca* associated fungus *A. versicolor* 16F-11. Although structural elucidations on the basis of room temperature NMR experiments could not resolve the structures of **1**, **2**, and **3**, the 1D and 2D NMR experiments carried out at −40 °C in CD_3OD for **2** and at 80 °C in DMSO-d_6 for **3**, respectively, resulted in the planar structures of **2** and **3** to be determined. For **1**, its structure was ascertained by theoretical NMR chemical shifts and ^{1}H NMR SSCCs studies of its two possible candidates elucidated from the 1D and 2D NMR spectra acquired at 80 °C in DMSO-d_6. Then, the absolute configurations of the enantiomers (+)-**1** and (−)-**1**, (+)-**2** and (−)-**2**, and (+)-**3** and (−)-**3** were elucidated with solution-state TDDFT ECD calculations. Concerning the paired ^{1}H NMR signals of **1**, **2**, and **3** appeared in solution, the calculated free energies of activation using the modified Eyring's equations based on VT ^{1}H-NMR study confirmed the hypothesis that the doubling of signals was due to the presence of two conformers separated by a relatively high energy barrier.

Experimental section

General procedures

Analytical thin-layer chromatography (TLC) systems were carried out on silica gel 60 F_{254} plates. ^{1}H, ^{13}C, DEPT135, COSY, HSQC, HMBC, NOESY, and ROESY NMR spectra were collected on an Agilent 600 MHz NMR instrument. UV and IR (film) spectra were recorded on a Hitachi U-3010 spectrophotometer and Jasco FTIR-400 spectrometer, respectively. Optical rotation measurements were conducted on a PerkinElmer model 341 polarimeter with a 10 cm length cell at room temperature. CD spectra were acquired on a Jasco J-715 spectropolarimeter at room temperature. HRESIMS spectra were determined on a Waters Xevo G2-XS QTOF spectrometer. HPLC-MS spectra were obtained using a Waters HPLC system equipped with a Waters Acquity QDa spectrometer and a Waters XBridge C18 column (Waters, 4.6 × 250 mm, 5 μm). Preparative MPLC was performed on an Interchim Puriflash 450 Instrument. Semi-preparative reversed-phased HPLC (RP-HPLC) was performed using a Waters 1525 pump equipped with a 2998 photodiode array detector and a Waters XBridge C18 column (Waters, 10 × 250 mm, 5 μm). Chiral HPLC separation was performed using CHIRALCEL OJ-RH column (150 × 4.6 mm, 5 μm).

Fungal material

The fungus *Aspergillus versicolor* 16F-11 was isolated from the inner tissue of the sponge *Phakellia fusca* collected from Yongxing Island, China and was identified by its rDNA amplification and sequence analysis of the ITS region (GenBank accession no. KM605199). A voucher specimen was deposited at

the School of Life Sciences and Biotechnology, Shanghai Jiao Tong University, Shanghai, China.

Culture, extraction, and isolation

Aspergillus versicolor 16F-11 was initially grown on PDA medium in a Petri dish for recovery (7 days). Its spores were directly inoculated into 250 mL Erlenmeyer flasks each containing 100 mL of the seed medium (potato 200 g L^{-1}, dextrose 20 g L^{-1}, and artificial seawater salts[27] 30 g L^{-1} in purified water) on a rotatory shaker (180 rpm) at 28 °C for 72 h. The subsequent expanded fermentation was proceeded in 54 × 2 L Erlenmeyer flasks. Each flask contained 6 g of sodium glutamate, 12 g of maltose, 12 g of mannitol, 12 g of $CaCO_3$, 6 g of glucose, 1.8 g of yeast extract, 0.6 g of corn syrup, 0.3 g of KH_2PO_4, 0.18 g of $MgSO_4 \cdot 7H_2O$, 18 g L^{-1} artificial seawater salts, and 600 mL of purified water, where 60 mL of the seed culture was transferred and incubated at 28 °C with shaking at 180 rpm for 12 days. The filtrated culture medium was extracted three times with EtOAc (30 L each) to afford a residue (3.0 g) after removal of the solvent under reduced pressure. The extract (3.0 g) was separated by reversed-phase MPLC (10–100% MeOH/H_2O, 180 min, flow rate 20 mL min^{-1}, UV detection at 210 nm) to afford twelve fractions (Fr.1–12). Subsequently, the fraction Fr.5 was purified by semi-ipreparative RP-HPLC (Waters XBridge C18 column (Waters, 10 × 250 mm, 5 μm), 35% MeCN/H_2O (2.0 mL min^{-1}, UV detection at 215 and 280 nm)) to yield versiorcinol B (**2**, 2.7 mg, t_R 40 min), versiorcinol C (**3**, 1.5 mg, t_R 46 min), and versiorcinol A (**1**, 2.0 mg, t_R 68 min).

(±)-Versiorcinol A (1). Colorless solid; UV (MeOH) λ_{max} (log ε) 221 (4.44), 279 (3.69) nm; IR (film) ν_{max} 3327, 2958, 2925, 2861, 1700, 1594, 1495, 1468, 1362, 1318, 1291, 1260, 1228, 1153, 1120, 1092, 1053, 1030, 997 cm^{-1}; ^1H and ^{13}C NMR data (DMSO-d_6 at 80 °C), see Table 1; HRESIMS *m*/*z* 365.1371 $[M + H]^+$ (calcd for $C_{22}H_{21}O_5$, 365.1389).

*(+)-**1**.* Colorless solid; $[\alpha]_D^{25}$ +45.9 (*c* 0.0027, MeOH); CD (3.38 × 10^{-4} M, MeOH), λ_{max} ($\Delta\varepsilon$) 208 (27.9), 277 (−3.40) nm.

*(−)-**1**.* Colorless solid; $[\alpha]_D^{25}$ −46.5 (*c* 0.0027, MeOH); CD (3.38 × 10^{-4} M, MeOH), λ_{max} ($\Delta\varepsilon$) 209 (−28.7), 277 (3.37) nm.

*(±)-Versiorcinol B (**2**).* Colorless solid; UV (MeOH) λ_{max} (log ε) 213 (4.45), 278 (3.53) nm; IR (film) ν_{max} 3329, 2926, 2857, 1700, 1658, 1599, 1468, 1361, 1319, 1289, 1259, 1148, 1054, 1026, 997 cm^{-1}; ^1H and ^{13}C NMR data (CD_3OD at −40 °C), see Table 1; HRESIMS *m*/*z* 347.1266 $[M + H]^+$ (calcd for $C_{22}H_{19}O_4$, 347.1283).

*(+)-**2**.* Colorless solid; $[\alpha]_D^{25}$ +37.6 (*c* 0.0029, MeOH); CD (3.61 × 10^{-4} M, MeOH), λ_{max} ($\Delta\varepsilon$) 214 (12.0), 270 (−1.83) nm.

*(−)-**2**.* Colorless solid; $[\alpha]_D^{25}$ −39.7 (*c* 0.0029, MeOH); CD (3.61 × 10^{-4} M, MeOH), λ_{max} ($\Delta\varepsilon$) 214 (−11.0), 276 (2.72) nm.

(±)-Versiorcinol C (3). Colorless solid; UV (MeOH) λ_{max} (log ε) 218 (4.48), 279 (3.66) nm; IR (film) ν_{max} 3328, 2924, 2856, 1700, 1619, 1596, 1496, 1467, 1423, 1323, 1288, 1259, 1217, 1147, 1055, 998 cm^{-1}; ^1H and ^{13}C NMR data (DMSO-d_6 at 80 °C), see Table 1; HRESIMS *m*/*z* 347.1266 $[M + H]^+$ (calcd for $C_{22}H_{19}O_4$, 347.1283).

*(+)-**3**.* Colorless solid; $[\alpha]_D^{25}$ +38.9 (*c* 0.0029, MeOH); CD (3.61 × 10^{-4} M, MeOH), λ_{max} ($\Delta\varepsilon$) 211 (20.5), 276 (−2.92) nm.

*(−)-**3**.* Colorless solid; $[\alpha]_D^{25}$ −39.9 (*c* 0.0029, MeOH); CD (3.61 × 10^{-4} M, MeOH), λ_{max} ($\Delta\varepsilon$) 208 (−23.6), 276 (3.37) nm.

Antibacterial activity assay

Racemates (±)-**1**, (±)-**2**, and (±)-**3** and enantiomers (+)-**1** and (−)-**1**, (+)-**2** and (−)-**2**, and (+)-**3** and (−)-**3** were evaluated for antibacterial activities against *Staphylococcus aureus* ATCC25923, methicillin-resistant *Staphylococcus aureus* ATCC43300, *Escherichia coli* ATCC25922, *Salmonella typhimurium* SL1344, *Acinetobacter baumanii* ATCC19606, *Klebsiella pneumoniae* ATCC13883, and *Enterococcus faecalis* C1129 in 96-well microplates according to a previously published protocol.[18,19,28] The final concentrations of each compound in the wells were 64, 32, 16, 8, 4, 2, 1, 0.5, 0.25, and 0.125 μg mL^{-1}. Chloramphenicol was used as the positive control and exhibited MICs of 4, 8, 4, 2, 32, 2, and 4 μg mL^{-1}, respectively, against the above mentioned bacteria.

Cytotoxicity assay

The cytotoxic activities of racemates (±)-**1**, (±)-**2**, and (±)-**3** and enantiomers (+)-**1** and (−)-**1**, (+)-**2** and (−)-**2**, and (+)-**3** and (−)-**3** against the human breast cancer cell MCF-7 and the lymphoma cell U937 were evaluated by the CCK-8 method as described previously.[29] The MCF-7 and U937 cell lines were obtained from the Institute of Biochemistry and Cell Biology (Shanghai, China).

Computational details

General procedure for chemical shifts and coupling constants calculations. Monte Carlo (MCMM) conformational searches were carried out by means of the Macromodel 9.9.223 (ref. 30) software using Merck Molecular Force Field (MMFF) applying a 21 kJ mol^{-1} energy window. The resulting conformers were subjected to geometry optimization using B3LYP/6-31G(d) with polarizable continuum model (PCM) for DMSO level of theory (Gaussian 09 (ref. 31)). After dereplication, the reoptimized conformers were further submitted to calculate NMR chemical shifts at B3LYP/6-311+G(2d,p) level using PCM model for DMSO and SSCCs using the DU8 basis set[24b] (Gaussian 09). Boltzmann distributions were estimated from the B3LYP/6-31G(d) or B3LYP/6-311+G(2d,p) relative thermal free energies (ΔG) in the PCM model for DMSO calculation at 353.15 K.

Empirical scaling of computed ^{13}C NMR chemical shifts. Computed chemical shifts were scaled empirically[32] according to

$$\delta_{\text{scaled}}{}^{x} = \frac{\delta_{\text{calcd}}{}^{x} - \text{intercept}}{\text{slope}},$$

where $\delta_{\text{calcd}}{}^{x}$ is the calculated chemical shift *x* (in ppm) relative to tetramethylsilane (TMS), which is calculated at the same level of theory, and slope and intercept are the slope and intercept resulting from a regression calculation on a plot of δ_{calcd} against δ_{exptl}.

General procedure for TDDFT ECD calculations. Monte Carlo (MCMM) conformational searches were carried out by

means of the Macromodel 9.9.223 software using Merck Molecular Force Field (MMFF) applying a 21 kJ mol^{-1} energy window. Geometry reoptimizations of the resultant conformers (B3LYP/6-31G(d) with PCM for CH_3OH level of theory) and TDDFT calculations (using various functionals (B3LYP, BH&HLYP, PBE0, CAM-B3LYP) and TZVP basis set) were performed with Gaussian 09. Boltzmann distributions were estimated from the B3LYP/6-31G(d) relative thermal free energies (ΔG) in the PCM/MeOH model calculations. In a preliminary set of calculations with versiorcinol A (**1**), the ECD spectra, calculation at B3LYP/TZVP level in MeOH (PCM), give the best agreement with the experimental one; therefore, this level of theory was used in all the subsequent TDDFT calculations. The ECD spectra were generated using the program SpecDis[33] by applying a Gaussian band shape with the width of 0.35 eV, from dipole-length rotational strengths. The MOLEKEL[34] software package was used for visualization of the results.

Conflicts of interest

There are no conflicts of interest to declare.

Acknowledgements

This research was supported by the National Natural Science Fund for Distinguished Young Scholars of China (81225023), the National Natural Science Fund of China (No. 41476121, 81402844, 81502936, 31600014, 41406139), the National High Technology Research and Development Program of China (863 Project, No. 2013AA092902), the Fund of the Science and Technology Commission of Shanghai Municipality (No. 15431900900), the Beijing Medical Award Foundation (No. YJHYXKYJJ-125).

Notes and references

1 P. Spiteller, *Nat. Prod. Rep.*, 2015, **32**, 971.
2 J. W. Blunt, B. R. Copp, R. A. Keyzers, M. H. Munro and M. R. Prinsep, *Nat. Prod. Rep.*, 2015, **32**, 116.
3 T. Bunyapaiboonsri, S. Yoiprommarat, K. Intereya and K. Kocharin, *Chem. Pharm. Bull.*, 2007, **55**, 304.
4 M. Chen, C.-L. Shao, X.-M. Fu, R.-F. Xu, J.-J. Zheng, D.-L. Zhao, Z.-G. She and C.-Y. Wang, *J. Nat. Prod.*, 2013, **76**, 547.
5 H. Gao, L. Zhou, S. Cai, G. Zhang, T. Zhu, Q. Gu and D. Li, *J. Antibiot.*, 2013, **66**, 539.
6 X. Wang, Y. Mou, J. Hu, N. Wang, L. Zhao, L. Liu, S. Wang and D. Meng, *Chem. Biodiversity*, 2014, **11**, 133.
7 S.-S. Hu, N. Jiang, X.-L. Wang, C.-J. Chen, J.-Y. Fan, G. Wurin, H.-M. Ge, R.-X. Tan and R.-H. Jiao, *Tetrahedron Lett.*, 2015, **56**, 3894.
8 O. I. Zhuravleva, N. N. Kirichuk, V. A. Denisenko, P. S. Dmitrenok, E. A. Yurchenko, E. M. Min′ko, E. V. Ivanets and S. S. Afiyatullov, *Chem. Nat. Compd.*, 2016, **52**, 227.
9 X.-M. Hou, C.-Y. Wang, Z.-G. She, Y.-C. Gu and C.-L. Shao, *Chem. Nat. Compd.*, 2016, **52**, 478.
10 Z.-H. Wu, Y.-R. Wang, D. Liu and P. Proksch, *Tetrahedron*, 2016, **72**, 50.
11 (*a*) S. Zenitani, S. Tashiro, K. Shindo, K. Nagai, K. Suzuki and M. Imoto, *J. Antibiot.*, 2003, **56**, 617; (*b*) S. Zenitani, K. Shindo, S. Tashiro, M. Sekiguchi, M. Nishimori, K. Suzuki and M. Imoto, *J. Antibiot.*, 2003, **56**, 658.
12 J. F. Sanchez, Y. M. Chiang, E. Szewczyk, A. D. Davidson, M. Ahuja, C. Elizabeth Oakley, J. Woo Bok, N. Keller, B. R. Oakley and C. C. Wang, *Mol. BioSyst.*, 2010, **6**, 587.
13 F.-Y. Du, X.-M. Li, J.-Y. Song, C.-S. Li and B.-G. Wang, *Helv. Chim. Acta*, 2015, **97**, 973.
14 V. Schroeckh, K. Scherlach, H. W. Nützmann, E. Shelest, W. Schmidt-Heck, J. Schuemann, K. Martin, C. Hertweck and A. A. Brakhage, *Proc. Natl. Acad. Sci. U. S. A.*, 2009, **106**, 14558.
15 Y. Li, W. Chang, M. Zhang, X. Li, Y. Jiao and H. Lou, *PLoS One*, 2015, **10**, e0128693.
16 M. Kawatani, H. Okumura, K. Honda, N. Kanoh, M. Muroi, N. Dohmae, M. Takami, M. Kitagawa, Y. Futamura, M. Imoto and H. Osada, *Proc. Natl. Acad. Sci. U. S. A.*, 2008, **105**, 11691.
17 A. Satou, T. Morishita, T. Hosoya and Y. Ishikawa, Japanese patent application JP11001480, 1999.
18 L.-J. Ding, B.-B. Gu, W.-H. Jiao, W. Yuan, Y.-X. Li, W.-Z. Tang, H.-B. Yu, X.-J. Liao, B.-N. Han, Z.-Y. Li, S.-H. Xu and H.-W. Lin, *Mar. Drugs*, 2015, **13**, 5579.
19 L.-J. Ding, W. Yuan, X.-J. Liao, B.-N. Han, S.-P. Wang, Z.-Y. Li, S.-H. Xu, W. Zhang and H.-W. Lin, *J. Nat. Prod.*, 2016, **79**, 2045.
20 R. Ditchfield, *Mol. Phys.*, 1974, **27**, 789.
21 (*a*) M. W. Lodewyk, M. R. Siebert and D. J. Tantillo, *Chem. Rev.*, 2012, **112**, 1839; (*b*) P. H. Willoughby, M. J. Jansma and T. R. Hoye, *Nat. Protoc.*, 2014, **9**, 643.
22 S. G. Smith and J. M. Goodman, *J. Am. Chem. Soc.*, 2010, **132**, 12946.
23 Use of the DP4 analysis is quite practical, owing to a versatile Java applet that the Goodman group has made available online, URL, http://www.jmg.ch.cam.ac.uk/tools/nmr/nmrParameters.html.
24 (*a*) A. G. Kutateladze and O. A. Mukhina, *J. Org. Chem.*, 2014, **79**, 8397; (*b*) A. G. Kutateladze and O. A. Mukhina, *J. Org. Chem.*, 2015, **80**, 5218.
25 Though we use two different DFT theory level for ΔG energies (B3LYP/6-311+G(2d,p) with PCM for DMSO at 353.15 K; B3LYP/6-31G(d) with PCM for DMSO at 353.15 K), increasing the basis set did not reduce the differences between calculated and experimental data (ESI, Tables S3–S5†). This anomaly and the small differences between measured and theoretical values are possibly due to imperfect conformer weightings in the DFT calculations (see ref. 24).
26 H. Shanan-Atidi and K. H. Bar-Eli, *J. Phys. Chem.*, 1970, **74**, 961.
27 D. R. Kester, I. W. Duedall, D. N. Connors and R. M. Pytkowicz, *Limnol. Oceanogr.*, 1967, **12**, 176.
28 Z. G. Khalil, R. Raju, A. M. Piggott, A. A. Salim, A. Blumenthal and R. J. Capon, *J. Nat. Prod.*, 2015, **78**, 949.

29 W.-Z. Tang, Z.-Z. Yang, F. Sun, S.-P. Wang, F. Yang and H.-W. Lin, *J. Asian Nat. Prod. Res.*, 2016, 691.
30 MacroModel, Schrödinger LLC, 2012, http://www.schrodinger.com/productpage/14/11/.
31 M. J. Frisch, G. W. Trucks, H. B. Schlegel, G. E. Scuseria, M. A. Robb, J. R. Cheeseman, G. Scalmani, V. Barone, B. Mennucci, G. A. Petersson, H. Nakatsuji, M. Caricato, X. Li, H. P. Hratchian, A. F. Izmaylov, J. Bloino, G. Zheng, J. L. Sonnenberg, M. Hada, M. Ehara, K. Toyota, R. Fukuda, J. Hasegawa, M. Ishida, T. Nakajima, Y. Honda, O. Kitao, H. Nakai, T. Vreven, J. A. Montgomery, J. E. Peralta Jr, F. Ogliaro, M. Bearpark, J. J. Heyd, E. Brothers, K. N. Kudin, V. N. Staroverov, R. Kobayashi, J. Normand, K. Raghavachari, A. Rendell, J. C. Burant, S. S. Iyengar, J. Tomasi, M. Cossi, N. Rega, J. M. Millam, M. Klene, J. E. Knox, J. B. Cross, V. Bakken, C. Adamo, J. Jaramillo, R. Gomperts, R. E. Stratmann, O. Yazyev, A. J. Austin, R. Cammi, C. Pomelli, J. W. Ochterski, R. L. Martin, K. Morokuma, V. G. Zakrzewski, G. A. Voth, P. Salvador, J. J. Dannenberg, S. Dapprich, A. D. Daniels, O. Farkas, J. B. Foresman, J. V. Ortiz, J. Cioslowski and D. J. Fox, *Gaussian 09, revision B.01*, Gaussian, Inc., Wallingford, CT, 2010.
32 G. Barone, L. Gomez-Paloma, D. Duca, A. Silvestri, R. Riccio and G. Bifulco, *Chem.–Eur. J.*, 2002, **8**, 3233.
33 T. Bruhn, Y. Hemberger, A. Schaumlöffel and G. Bringmann, *SpecDis version 1.50*, University of Wuerzburg, Germany, 2010.
34 U. Varetto, *MOLEKEL 5.4.*,Swiss National Supercomputing Centre, Manno, Switzerland, 2009.